SEMI-AUTONOMOUS AVOIDANCE OF MOVING HAZARDS FOR PASSENGER VEHICLES

Sterling J Anderson
Department of Mechanical Engineering
Massachusetts Institute of Technology
Cambridge, MA 02139
ster@mit.edu

Steven C. Peters
Department of Mechanical Engineering
Massachusetts Institute of Technology
Cambridge, MA 02139
scpeters@mit.edu

Tom E. Pilutti
Ford Research Laboratories
Ford Motor Co.
Dearborn, MI 48124
tpilutti@ford.com

H. Eric Tseng
Ford Research Laboratories
Ford Motor Co.
Dearborn, MI 48124
htseng@ford.com

Karl Iagnemma
Dept of Mechanical Engineering
Massachusetts Institute of Tech
Cambridge, MA 02139
kdi@mit.edu

ABSTRACT

This paper presents a method for semi-autonomous hazard avoidance in the presence of unknown moving obstacles and unpredictable driver inputs. This method iteratively predicts the motion and anticipated intersection of the host vehicle with both static and dynamic hazards and excludes projected collision states from a traversable corridor. A model predictive controller iteratively replans a stability-optimal trajectory through the navigable region of the environment while a threat assessor and semi-autonomous control law modulate driver and controller inputs to maintain stability, preserve controllability, and ensure safe hazard avoidance. The efficacy of this approach is demonstrated through both simulated and experimental results using a semi-autonomously controlled Jaguar S-Type.

INTRODUCTION

Recent traffic safety reports from the National Highway Traffic and Safety Administration show that in 2007 alone, over 41,000 people were killed and another 2.5 million injured in motor vehicle accidents in the United States [1]. The longstanding presence of passive safety systems in motor vehicles, combined with the ever-increasing influence of active systems, has contributed to a decline in these numbers from previous years. Still, the opportunity for improved collision avoidance technologies remains significant.

Recent developments in onboard sensing, lane detection, obstacle recognition, and drive-by-wire capabilities have facilitated active safety systems that autonomously or semi-autonomously assist in the driving task [2]. In addition to avoiding static hazards, these systems must account for the motion of dynamic roadway hazards in the presence of uncertain sensor data and unpredictable hazard motion. This consideration, while challenging in its own right, is compounded in semi-autonomous vehicle systems, in which a human operator maintains at least partial control of the host vehicle. In these scenarios, the trajectory planner and semi-autonomous controller must allow for (and reject if necessary) unanticipated vehicle state and input disturbances caused by the human operator.

In the traditional approach to autonomous vehicle navigation, a path planner and controller are arranged as a tiered subsystem, with a planner designing a collision-free path and the controller seeking to track that path while rejecting disturbances. Common path planning approaches include rapidly-exploring random trees [3], graph search methods [4], potential fields analysis [5], velocity obstacles [6], and neural optimization techniques [7]. Control laws commonly employed in these systems include PID schemes [8], linear-quadratic regulators [9], and nonlinear fuzzy controllers [10].

With a human driver in the loop, tiered subsystem architectures that rely on a pre-planned path may be overly restrictive at best and inaccurate at worst. By seeking to limit the vehicle trajectory to a specific path, these approaches neither allow nor account for deviations from the nominal trajectory caused by human inputs or unanticipated hazard motion. Many existing semi-autonomous systems also seek to perform the hazard avoidance task without explicitly accounting for the effect of driver inputs on the vehicle trajectory [11]. These systems generally estimate the threat posed by static or moving hazards

with simple time-based, distance-based, or deceleration-based measures [12-15]. While these metrics provide a useful estimate of threat posed by a given maneuver, they are poorly suited to consider multiple hazards, complex vehicle dynamics, actuator and controller limitations, or complicated environmental geometry with its attendant constraints.

In [16], a framework for semi-autonomous control of passenger vehicles is presented. This framework uses Model Predictive Control (MPC) to iteratively plan trajectories through a traversable corridor, assess the threat this trajectory poses to the vehicle, and regulate driver and controller inputs to prevent that threat from exceeding a given threshold. In the context of static hazards, this system's model-based threat assessment provides an efficient means of: 1) combining static roadway hazards such as lane boundaries and roadway obstacles into realistic spatial constraints and 2) combining these constraints with knowledge of the vehicle dynamics to predict the threat posed by those hazards given the current inputs of a human driver.

This paper extends this framework's hazard avoidance capabilities to account for both static and dynamic hazards and demonstrates (via simulation and experiment) the advantages of this approach over other planning and control techniques designed to avoid static and moving obstacles. Basic framework operation is first presented, followed by a description of the method used to predict the future position of moving roadway hazards, assess the threat each of these hazards poses, and avoid them semi-autonomously. Simulation setup and results are then presented, followed by experimental setup and results, and the paper closes with general conclusions.

FRAMEWORK DESCRIPTION

The framework described in this paper leverages the predictive and constraint-handling capabilities of MPC to perform trajectory planning, threat assessment, and semi-autonomous hazard avoidance. First, an objective function is established to capture desirable performance characteristics of a safe or "optimal" vehicle path. Boundaries tracing the edges of the drivable road surface are derived from (assumed) forward-looking sensor data and a higher-level corridor planner. These boundaries extrapolate the current state of road hazards (vehicles, pedestrians, etc.) to establish a traversable corridor constraining the vehicle's projected lateral position. This constraint data, together with a model of the vehicle dynamics is then used to calculate an optimal sequence of inputs and the associated vehicle trajectory. The predicted trajectory is treated as a "best-case" scenario and used to establish the minimum threat posed to the vehicle given its current state and a series of best-case inputs. This threat is then used to calculate the intervention required to prevent departure from the traversable corridor and driver/controller inputs are scaled accordingly. Figure 1 shows a block diagram of this system.

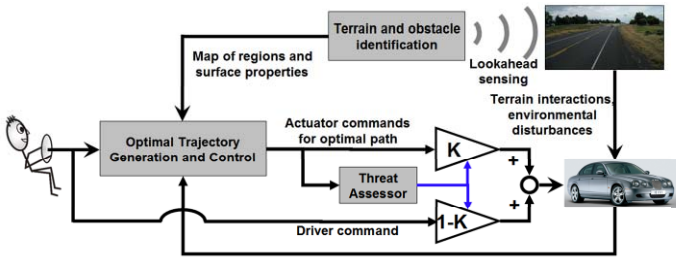

FIGURE 1. DIAGRAM OF AN ACTIVE SAFETY SYSTEM

Assumptions

In this paper it is assumed that road lane data is available and that the instantaneous position, velocity, and acceleration of road hazards have been measured or estimated by on-board sensors or vehicle-to-vehicle communication. Existing systems and previous work in onboard sensing and sensor fusion justify this as a reasonable assumption [17]. Radar, LIDAR, and vision-based lane-recognition systems [3], along with various sensor fusion approaches [18] have been proposed to provide the lane, hazard, and environmental information needed by this framework. Where multiple corridor options exist (such as cases where the roadway branches or the vehicle must avoid an obstacle in the center of the lane), it is assumed that a high-level path planner has selected a single corridor through which the vehicle should travel.

Path Planning

The best-case (or baseline) path through the constrained corridor is predicted by an MPC controller. Model Predictive Control is a finite-horizon optimal control scheme that uses a model of the plant to predict future vehicle state evolution and optimize a set of inputs such that this prediction satisfies constraints and minimizes a user-defined objective function. At each time step, t, the current plant state is sampled and a cost-minimizing control sequence spanning from time t to the end of a control horizon of n sampling intervals, $t+n\Delta t$, is computed subject to inequality constraints. The first element in this input sequence is implemented at the current time and the process is repeated at subsequent time steps. Three important elements of the controller implemented in this paper – the plant model, objective function, and constraint setup – are described below.

Vehicle Dynamic Model. The vehicle model used by the controller consists of the linearized kinematics of a 4-wheeled vehicle along with its lateral (wheel slip) and yaw dynamics. Vehicle states include the position of its center of gravity [x, y], the vehicle yaw angle ψ, yaw rate $\dot{\psi}$, and sideslip angle β, as illustrated in Figure 2. The input to the system is the front steer angle δ.

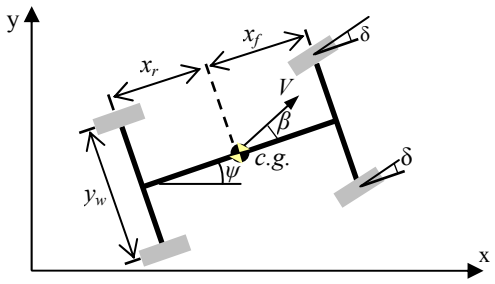

FIGURE 2. VEHICLE MODEL USED IN MPC CONTROLLER

Table 1 defines and quantifies this model's parameters.

TABLE 1. VEHICLE MODEL PARAMETERS

Symbol	Description	Value [units]
m	Total vehicle mass	2050 [kg]
I_{zz}	Yaw moment of inertia	3344 [kg m^2]
x_f	C.g. distance to front wheels	1.43 [m]
x_r	C.g. distance to rear wheels	1.47 [m]
y_w	Track width	1.44 [m]
C_f	Front cornering stiffness	1433 [N/deg]
C_r	Rear cornering stiffness	1433 [N/deg]
μ	Surface friction coefficient	1

Tire compliance is included in the model by approximating lateral tire force (F_y) as the product of wheel cornering stiffness (C) and wheel sideslip (α or β) as in

$$F_y = C\alpha \tag{1}$$

and illustrated in Figure 2.

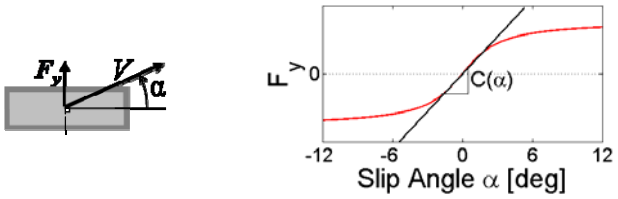

FIGURE 3. TIRE COMPLIANCE MODEL ILLUSTRATING VELOCITY V, SLIP ANGLE α, AND LATERAL FORCE F_Y

Linearizing about a constant speed and assuming small slip angles, equations of motion for this model become (where δ represents the steering angle input),

$$\begin{aligned} \dot{x} &= V \\ \dot{y} &= V(\psi + \beta) \\ \dot{\beta} &= \frac{-(C_r + C_f)}{mV}\beta + \left(\frac{(C_r x_r - C_f x_f)}{mV^2} - 1\right)\dot{\psi} + \frac{C_f}{mV}\delta \\ \ddot{\psi} &= \frac{(C_r x_r - C_f x_f)}{I_{zz}}\beta - \frac{(C_r {x_r}^2 + C_f {x_f}^2)}{I_{zz}V}\dot{\psi} + \frac{C_f x_f}{I_{zz}}\delta \end{aligned} \tag{2}$$

where C_f and C_r represent the (linearized) cornering stiffness of the lumped front wheels and the lumped rear wheels, and x_f and x_r are the longitudinal distance from the c.g. of the front and rear wheels, respectively. As described in [19] and briefly discussed below, small slip angles are maintained by configuring the MPC objective function and semi-autonomous intervention law to keep wheel slip within the roughly linear range of the tire force curve. The constant speed assumption used in this linearization reflects the common driver intention in highway driving scenarios.

Constraint Setup. Assuming that the environment has been delineated previously (see assumptions above), the boundaries of the traversable road surface ($y_{\min}(x)$ and $y_{\max}(x)$) are sampled over the prediction horizon to generate the constraint vectors

$$\begin{aligned} \mathbf{y}^{y}{}_{\max}(k) &= \left[y^{y}{}_{\max}(k+1) \quad \cdots \quad y^{y}{}_{\max}(k+p)\right]^T \\ \mathbf{y}^{y}{}_{\min}(k) &= \left[y^{y}{}_{\min}(k+1) \quad \cdots \quad y^{y}{}_{\min}(k+p)\right]^T \end{aligned} \tag{3}$$

Moving hazards are considered in the autonomous control problem by estimating their future position based on their current position, velocity, and (optionally) acceleration and excluding predicted collision states from the constraint-bounded corridor. In the simulation results shown below, untraversable regions representing obstacles moving in one dimension (results may be generalized to 2-dimensional motion) were incorporated into time-varying corridors as follows:

Given a (constant) host velocity $\dot{x}_{host}$ and obtaining the current velocity of roadway hazards $\dot{x}_{haz}$ from tracking sensors or vehicle-to-vehicle communication, where $x_{host}(t)$ and $x_{haz}(t)$ represent the current position of the host and hazard, respectively at time t, the estimated time to collision Δt_c evaluated at time t0 is given by

$$\Delta t_c\big|_{t_0} = t_c - t_0 = \begin{cases} -\dfrac{\tilde{x}(t_0)}{\dot{\tilde{x}}(t_0)} & \begin{cases} \text{for } \dot{\tilde{x}}(t_0) < 0, \;\; \tilde{x}(t_0) > 0 \\ \text{or } \dot{\tilde{x}}(t_0) > 0, \;\; \tilde{x}(t_0) < 0 \end{cases} \\ \pm\infty & \begin{cases} \text{for } \dot{\tilde{x}}(t_0) < 0, \;\; \tilde{x}(t_0) < 0 \\ \text{or } \dot{\tilde{x}}(t_0) = 0 \end{cases} \end{cases} \tag{4}$$

to first order where $\dot{\tilde{x}}(t) = \dot{x}_{haz}(t) - \dot{x}_{host}$, $\tilde{x}(t) = x_{haz}(t) - x_{host}(t)$, or

$$\Delta t_c\big|_{t_0} = \begin{cases} \dfrac{-\dot{\tilde{x}}(t_0) - \sqrt{\dot{\tilde{x}}^2(t_0) - 2\ddot{x}_{haz}(t_0)\cdot\tilde{x}(t_0)}}{\ddot{x}_{haz}} & \begin{cases} \text{for } \ddot{x}_{haz}(t_0) \neq 0, \;\; \dot{\tilde{x}}(t_0) < 0 \\ \text{or } \ddot{x}_{haz}(t_0) < 0, \;\; \dot{\tilde{x}}(t_0) \geq 0 \end{cases} \\ -\dfrac{\tilde{x}(t_0)}{\dot{\tilde{x}}(t_0)} & \text{for } \ddot{x}_{haz}(t_0) = 0, \;\; \dot{\tilde{x}}(t_0) < 0 \\ \pm\infty & \begin{cases} \text{for } \ddot{x}_{haz}(t_0) > 0, \;\; \dot{\tilde{x}}(t_0) \geq 0 \\ \text{or } \ddot{x}_{haz}(t_0) = 0, \;\; \dot{\tilde{x}}(t_0) \geq 0 \end{cases} \end{cases} \tag{5}$$

to second-order (requiring that $\tilde{x}(t_0) \geq 0$ in (5)).

Given $\Delta t_c\big|_{t_0}$, the x position of each road hazard at t_c is then estimated as

$$x_{haz}\left(t_c\big|_{t_0}\right) = x_{haz}(t_0) + \dot{x}_{haz}(t_0)\cdot \Delta t_c\big|_{t_0} \tag{6}$$

or

$$x_{haz}\left(t_c\big|_{t_0}\right) = x_{haz}(t_0) + \dot{x}_{haz}(t_0)\cdot \Delta t_c\big|_{t_0} + \frac{1}{2}\ddot{x}_{haz}(t_0)\cdot \Delta t_c\big|_{t_0}^{\,2} \tag{7}$$

to first- and second-order, respectively. Hazard depth from the host vehicle's perspective is then estimated by

$$\Delta x_{haz}\left(t_c\big|_{t_0}\right) \approx \Delta x_{haz}(t_0) - \dot{x}_{haz}(t_0)\cdot\left(\Delta x_{haz}(t_0)/\dot{\tilde{x}}(t_0)\right) \tag{8}$$

assuming some knowledge of the true hazard depth (Δx_{haz}).

Constraints on vehicle position are constructed at each sampling instant to form a convex (in y) corridor from the outline of each hazard's anticipated position and depth at time t_c. Figure 4 illustrates what a snapshot of this time-varying constraint placement might look like to the controller.

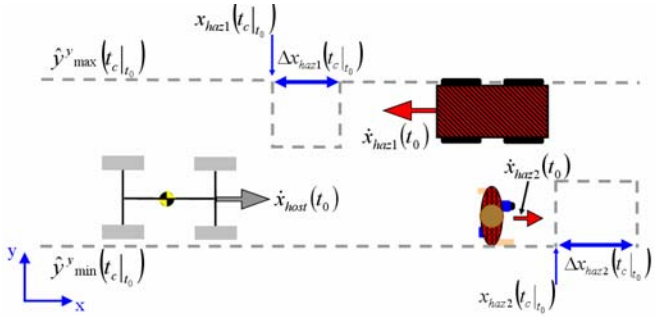

FIGURE 4. ILLUSTRATION OF CONSTRAINT PLACEMENT (Y^{Y}_{MAX}, Y^{Y}_{MIN}) FOR MOVING HAZARDS

Notice that the constraint "shadow" cast by a hazard moving in the opposite direction as the host vehicle appears shallower than the hazard's true depth. Similarly, the shadow cast by a hazard moving in the same direction as the host vehicle is effectively deepened.

By enforcing vehicle position constraints at the boundaries of the traversable environment*, the controller forces the MPC-generated path to remain within the constraint-bounded corridor whenever dynamically feasible. Coupling this lateral position constraint with input constraints $u_{min/max}$, input rate constraints $\Delta u_{min/max}$, and vehicle dynamic considerations, the traversable operating corridor delineated by y^{y}_{max} and y^{y}_{min} translates to a safe operating region within the state space.

Objective Function. Inside the constraint-bounded tube, various vehicle outputs may be minimized to improve vehicle performance, stability, and controllability. In this work, front wheel sideslip ($\alpha = (x_f/V)\dot{\psi} + \beta - \delta$) is chosen for its influence on the controllability of front-wheel-steered vehicles. As illustrated in Figure 3, cornering friction begins to decrease above critical slip angles. These critical angles are well-known and provide a direct mapping from environmental conditions to vehicle handling limitations. The linearized tire compliance model's failure to account for this decrease further motivates the suppression of front wheel slip angles to reduce controller-plant model mismatch. In [20] it is shown that limiting tire slip angle to avoid this strongly nonlinear (and possibly unstable) region of the tire force curve can significantly enhance vehicle stability. Finally, trajectories that minimize wheel slip also tend to minimize lateral acceleration and yaw rates, leading to a safer and more comfortable ride.

Describing the discretized vehicle plant model by

$$\mathbf{x}_{k+1} = \mathbf{A}\mathbf{x}_k + \mathbf{B}_u\mathbf{u}_k + \mathbf{B}_v\mathbf{v}_k \tag{9}$$

$$\mathbf{y}_k = \mathbf{C}\mathbf{x}_k + \mathbf{D}_v\mathbf{v}_k \tag{10}$$

with **x, y, u,** and **v** representing states, outputs, inputs, and disturbances respectively, a quadratic objective function over a prediction horizon of p sampling intervals is defined as

$$J_k = \sum_{i=k+1}^{k+p}\frac{1}{2}\mathbf{y}_i{}^{\mathrm{T}}\mathbf{R}_y\mathbf{y}_i + \sum_{i=k}^{k+p-1}\frac{1}{2}\mathbf{u}_i{}^{\mathrm{T}}\mathbf{R}_u\mathbf{u}_i + \sum_{i=k}^{k+p-1}\frac{1}{2}\Delta\mathbf{u}_i{}^{\mathrm{T}}\mathbf{R}_{\Delta u}\Delta\mathbf{u}_i + \frac{1}{2}\rho_\varepsilon\varepsilon^2 \tag{11}$$

where $\mathbf{R}_y$, $\mathbf{R}_u$, and $\mathbf{R}_{\Delta u}$ represent diagonal weighting matrices penalizing deviations from $\mathbf{y}_i = \mathbf{u}_i = \Delta\mathbf{u}_i = 0$, ρ_ε represents the penalty on constraint violations, n denotes the number of free control moves, and ε represents the maximum constraint violation over the prediction horizon p. Inequality constraints on vehicle position (**y**), inputs (**u**), and input rates (**Δu**) are then defined as:

$$\begin{gathered}
\mathbf{y}^j{}_{\min}(i) - \varepsilon\mathbf{V}^j{}_{\min}(i) \le \mathbf{y}^j(k+i+1\,|\,k) \le \mathbf{y}^j{}_{\max}(i) + \varepsilon\mathbf{V}^j{}_{\max}(i) \\
\mathbf{u}^j{}_{\min}(i) \le \mathbf{u}^j(k+i+1\,|\,k) \le \mathbf{u}^j{}_{\max}(i) \\
\Delta\mathbf{u}^j{}_{\min}(i) \le \Delta\mathbf{u}^j(k+i+1\,|\,k) \le \Delta\mathbf{u}^j{}_{\max}(i) \\
i = 0,\ldots,\, p-1 \\
\varepsilon \ge 0
\end{gathered} \tag{12}$$

where the vector **Δu** represents the change in input from one sampling instant to the next, the superscript "$(\bullet)^j$" represents the j^{th} component of a vector, k represents the current time, and the notation $(\bullet)^j(k+i|k)$ denotes the value predicted for time $k+i$ based on the information available at time k. The vector **V** allows for variable constraint softening over the prediction horizon, p, when ε is included in the objective function. Table 2 defines and quantifies this controller parameters used in this paper.

TABLE 2. CONTROLLER PARAMETERS

Symbol	Description	Value [units]
$[\Phi_{eng}\ \Phi_{aut}]$	Semi-autonomous intervention thresholds	[0 3] deg
p	Prediction horizon	40
n	Control horizon	20
$R_y^{(\alpha)}$	Weight on front wheel slip	0.2657
R_u	Weight on steering input	0.01
$R_{\Delta u}$	Weight on steering input rate ($\Delta/\Delta t$)	0.01
$u_{min/max}$	Constraint on steering input	± 10 deg
Δu_{min}	Constraint on steering input rate ($/\Delta t$)	± 0.75 deg
Δu_{max}		(15 deg/s)

* Position constraints may be applied to vehicle profile or offset and applied to its center of gravity. In this paper, the later approach was used. Results plots shown here illustrate the host vehicle c.g. traveling among the offset corridor.

y^{y}_{min} y^{y}_{max}	Lateral position constraints	Scenario dependent
ρ_{ε}	Weight on constraint violation	1×10^{5}
$\mathbf{V}$	Variable constraint relaxation on vehicle position	$\mathbf{V}(1...p\text{-}1) = 1.25$ $\mathbf{V}(p) = 0.01$
Δt	Controller timestep (update rate)	50 ms

Threat Assessment and Controller Intervention

Similar to the controller described in [16] the MPC controller used here constrains vehicle position, input magnitude, and input rates to satisfy safety requirements, while minimizing front wheel slip to maximize controllability and minimize plant-controller model mismatch. At each controller timestep, predicted front wheel sideslip ($\boldsymbol{\alpha}$) is converted to a scalar threat metric Φ by

$$\Phi(k) = \max\left(\alpha_{k+1} \quad \alpha_{k+2} \quad \cdots \quad \alpha_{k+p}\right). \tag{13}$$

This threat assessment is then used in a piecewise-linear intervention function $K(\Phi, u_{driver}, u_{MPC}) \in [0 \quad 1]$ to blend driver and controller inputs as

$$u_{vehicle} = K(\Phi)u_{MPC} + (1 - K(\Phi))u_{driver}. \tag{14}$$

The intervention function K used in (14) is parameterized by threshold threat values Φ_{eng} and Φ_{aut}. While predicted threat remains below Φ_{eng}, the driver maintains full control. As predicted threat increases, so does the proportion of control allocated to the controller. In the simulations and experiments shown below, K was calculated as

$$K = \begin{cases} 0 & 0 \le \Phi \le \Phi_{eng} \\ \dfrac{\Phi_{aut} - \Phi}{\Phi_{aut} - \Phi_{eng}} & \Phi_{eng} \le \Phi \le \Phi_{aut} \\ 1 & \Phi \ge \Phi_{aut} \end{cases} \tag{15}$$

To ensure that avoidance maneuvers remained within the roughly-linear region of the tire force curve (as assumed in the MPC model), Φ_{aut} was set at three degrees of front wheel slip.

SIMULATION STUDIES

Setup

Controller performance was simulated using a nonlinear ADAMS® model of a generic vehicle featuring a double wishbone suspension, passive roll stabilizers, and rack and pinion steering. Tire forces were approximated using a Pacejka tire model, which describes longitudinal and cornering forces as a function of normal force, tire slip angle, surface friction, and longitudinal slip. The vehicle model described by (2), with the parameters given in Table 1 was used in the receding horizon controller.

Results

Simulation results were obtained for various maneuvers, driver inputs, objective function configurations, and intervention laws. Results below are shown for scenarios in which the driver (traveling at a constant 20 m/s) does not take appropriate evasive action to avoid moving roadway hazards. In each case, the driver steer input (δ_{driver}) was set at zero to simulate an inattentive driver. In future testing, it is expected that nonzero driver inputs will lead to synergistic driver-controller interaction effects similar to those observed in [16]. Figure 5 shows the results of autonomous and semi-autonomous simulations.

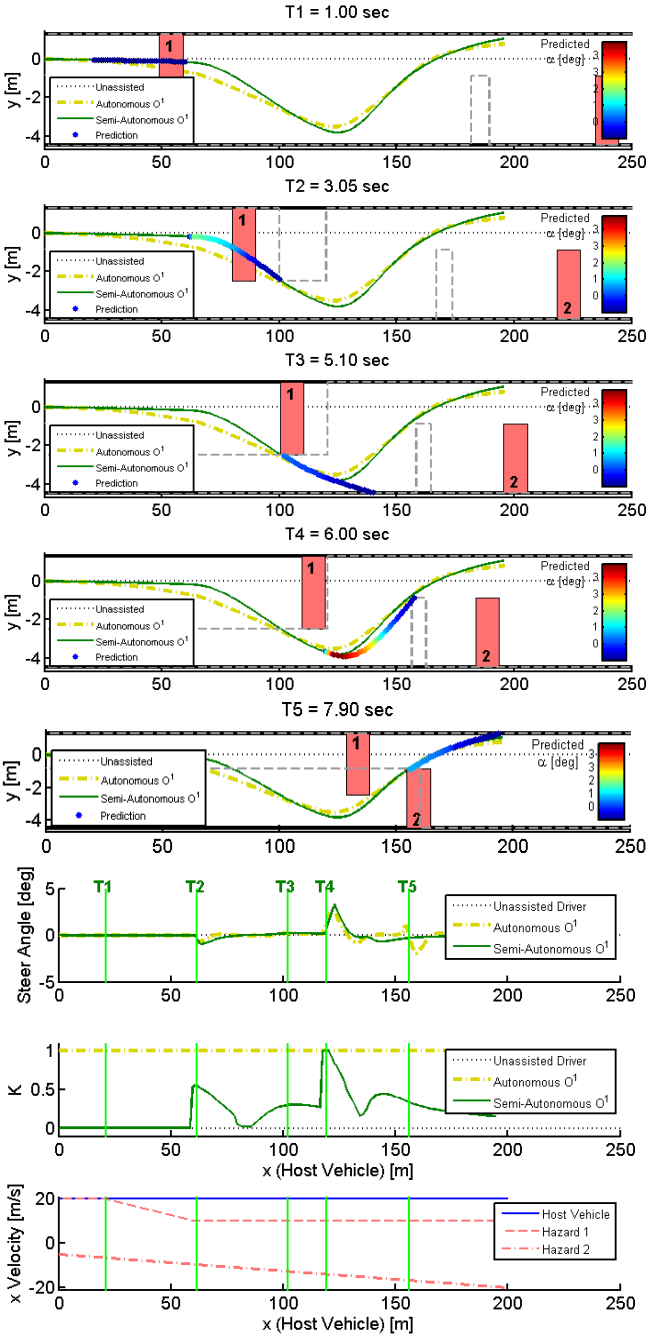

FIGURE 5. SIMULATION RESULTS COMPARING AUTONOMOUS AND SEMI-AUTONOMOUS CONTROLLER PERFORMANCE AMONG MOVING HAZARDS

In this scenario, the host vehicle initially trails obstacle 1 while both travel at 20 m/s. At T1, obstacle 1 begins to decelerate, prompting the host vehicle to begin a passing maneuver at T2. At T3, the host clears the first obstacle and "sees" an accelerating obstacle 2 in the oncoming lane at T4. Adjusting quickly in response to the heightened threat, the semi-autonomous controller takes complete control of the vehicle and successfully guides it safely past the hazard (whose projected area has been expanded to account for the geometry of the host vehicle). Note that by estimating the future position of each hazard using a first-order hold on its current state as in (4) and (6), the predicted collision time and location does not explicitly account for the acceleration of each hazard. Instead, it adjusts its estimate at each sampling instant based on the hazard's current velocity. This adjustment is apparent in Figure 5 as a shift in corridor boundaries as hazard velocity changes.

Figure 6 shows how the semi-autonomous controller's performance changes when future hazard positions are predicted to 2nd-order.

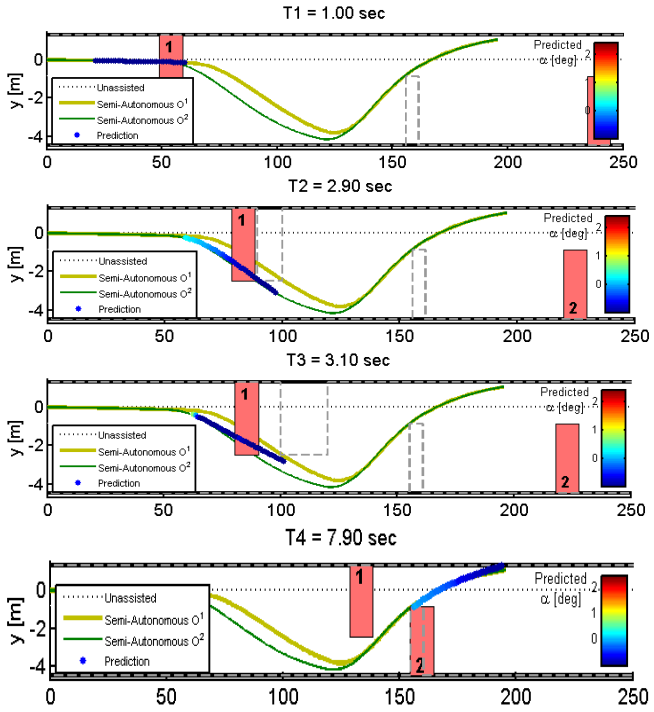

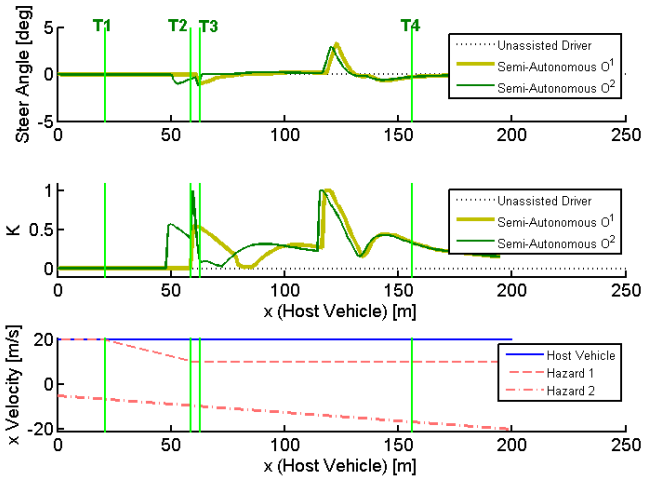

FIGURE 6. SIMULATION RESULTS COMPARING SEMI-AUTONOMOUS CONTROLLER PERFORMANCE AMONG MOVING HAZARDS USING A 1ST- AND 2ND-ORDER PREDICTIONS OF FUTURE HAZARD POSITION

Notice that just after T1, hazard 1 begins to decelerate, causing the controller to place its projected intersect with the hazard at x≈85 m. This prompts a sharp increase in controller intervention to avoid the slowing hazard. When hazard 1 stops its deceleration at T3, the controller extends the predicted intersection point and proceeds to successfully avoid the hazard. Finally, note that the predicted intersection with hazard 2 remains unchanged due to its constant acceleration throughout the scenario.

EXPERIMENTAL STUDIES

Setup

Experimental testing was performed using a Jaguar S-Type and multiple human drivers. Driver and actuator steering inputs were coupled via an Active Front Steer (AFS) system. An inertial and GPS navigation system was used to measure vehicle position, sideslip, yaw angle, and yaw rate while an 800 MHz dSPACE processor ran controller code and commanded steering actuators.

Results

The semi-autonomous framework proved capable of keeping the vehicle within the traversable corridor for each of the scenarios tested, with several human drivers, and multiple intervention laws. Additionally, the 50 ms control loop proved sufficient for control calculations. Figure 7 shows the results of two semi-autonomous experiments.

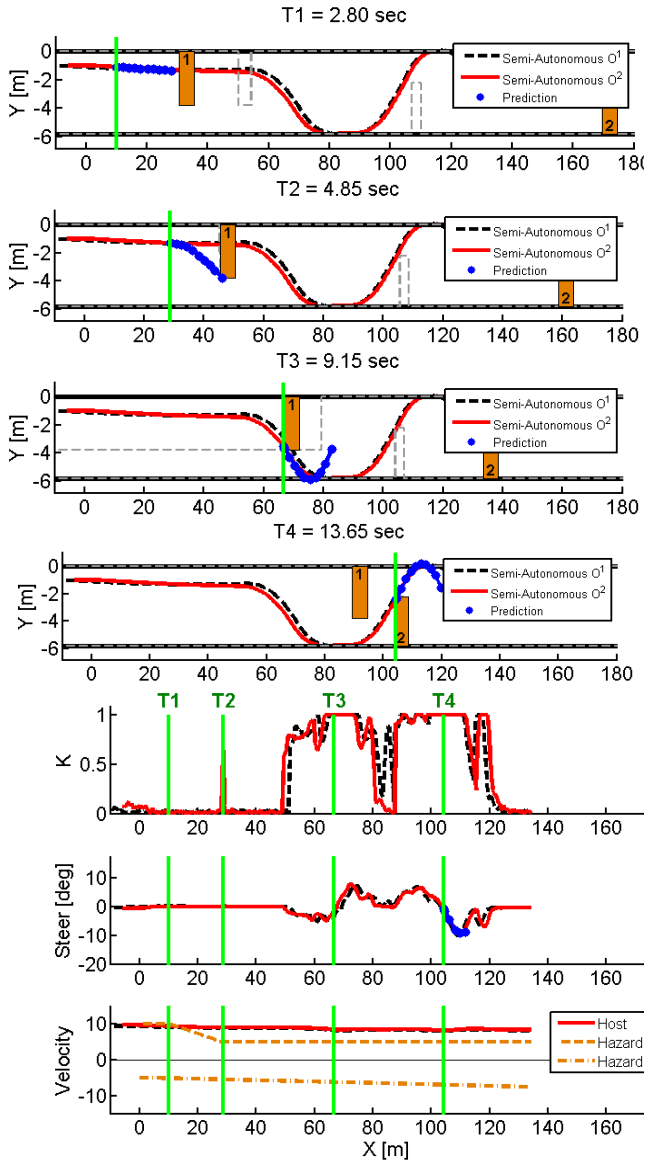

FIGURE 7. EXPERIMENTAL RESULTS OF SEMI-AUTONOMOUS CONTROLLERS NAVIGATING AMONG MOVING HAZARDS USING 1ST- AND 2ND-ORDER HAZARD POSITION PREDICTIONS

Notice in Figure 7 that the assumption of constant hazard acceleration used by the 2nd-order approximation causes a brief spike in controller intervention K at T2. Because this intervention is short-lived and multiplies a very small steer command, however, it does not significantly affect the vehicle trajectory. Once hazard 1 reaches a steady velocity, both predictions place the corridor boundary at $x \approx 65$ m and successfully avoid the hazard. Also notice that for this particular scenario, large predicted front wheel sideslip, combined with the driver's inaction, lead to significant controller intervention between T3 (once the host-facing facade of hazard 1 has been cleared) and T4 (once the oncoming facade of hazard 2 has been avoided and the vehicle has righted itself in the appropriate lane). This control is rapidly relinquished to the human driver as soon as hazard 2 has been avoided and lane departure averted.

CONCLUSION

This paper described a semi-autonomous hazard avoidance framework that performs trajectory planning, threat assessment, and shared-adaptive control among both static and dynamic hazards. While accounting for hazard motion is not particularly new or novel (unmanned aerial vehicle research has been accounting for hazard motion for years) [21], the integration of multiple static and dynamic obstacles, together with stability considerations and dynamic constraints into a compact corridor representation is relatively unexplored, particularly in the semi-autonomous ground vehicle applications. Moving hazards were factored into the constrained optimal control problem by predicting their position at intersection with the host vehicle and mapping this region into corridor-like constraints on the host vehicle's lateral position. This method was shown in simulation and experiment to efficiently avoid collisions with moving and stationary hazards while satisfying position, input, and dynamic vehicle constraints using both first- and second-order predictions of future hazard positions. Additionally, the framework was shown to provide significant autonomy to a human driver during low threat situations, intervening only as necessary to keep the vehicle within the traversable roadway corridor. Simulation and experimental results have also shown this control framework to be stable in the presence of system-inherent time delays, though a rigorous stability proof is a topic of current investigation. Further work is needed before this research is road-ready.

ACKNOWLEDGMENTS

The authors would like to thank Mitch McConnell, Dorian Spero, Jim Martell, Alex Miller, Tony Sleath, Gurunath Vemulakonda, Matt Rupp, Tim Zwicky, Jianbo Lu, Chris Teslak, Reid Steiger, and Jamil Alwan, all of Ford Motor Co. for their assistance in conducting the abovementioned experiments.

REFERENCES

[1] National Highway Traffic Safety Administration (NHTSA), *2007 Traffic Safety Annual Assessment - Highlights*, NHTSA National Center for Statistics and Analysis, 2008.

[2] M. Weilkes, L. Burkle, T. Rentschler, and M. Scherl, "Future vehicle guidance assistance - combined longitudinal and lateral control," *Automatisierungstechnik*, vol. 42, Jan. 2005, pp. 4-10.

[3] J. Leonard, J. How, S. Teller, M. Berger, S. Campbell, G. Fiore, L. Fletcher, E. Frazzoli, A. Huang, S. Karaman, O. Koch, Y. Kuwata, D. Moore, E. Olson, S. Peters, J. Teo, R. Truax, M. Walter, D. Barrett, A. Epstein, K. Maheloni, K. Moyer, T. Jones, R. Buckley, M. Antone, R. Galejs, S. Krishnamurthy, and J. Williams, "A perception-driven autonomous urban vehicle," *Journal of Field Robotics*, vol. 25, 2008, pp. 727-774.

[4] R. Vaidyanathan, C. Hocaoglu, T.S. Prince, and R.D. Quinn, "Evolutionary path planning for autonomous air vehicles using multiresolution path representation," *2001 IEEE/RSJ International Conference on Intelligent Robots and Systems, Oct 29-Nov 3 2001*, Maui, HI, United States: Institute of Electrical and Electronics Engineers Inc., 2001, pp. 69-76.

[5] E.J. Rossetter and J. Christian Gardes, "Lyapunov based performance guarantees for the potential field lane-keeping assistance system," *Journal of Dynamic Systems, Measurement and Control, Transactions of the ASME*, vol. 128, 2006, pp. 510-522.

[6] P. Fiorini and Z. Shiller, "Motion planning in dynamic environments using velocity obstacles," *International Journal of Robotics Research*, vol. 17, Jul. 1998, pp. 760-72.

[7] Dong Kwon Cho and Myung Jin Chung, "Intelligent motion control strategy for a mobile robot in the presence of moving obstacles," *Proceedings IROS '91. IEEE/RSJ International Workshop on Intelligent Robots and Systems '91. Intelligence for Mechanical Systems (Cat. No.91TH0375-6), 3-5 Nov. 1991*, New York, NY, USA: IEEE, 1991, pp. 541-6.

[8] L.B. Cremean, T.B. Foote, J.H. Gillula, G.H. Hines, D. Kogan, K.L. Kriechbaum, J.C. Lamb, J. Leibs, L. Lindzey, C.E. Rasmussen, A.D. Stewart, J.W. Burdick, and R.M. Murray, "Alice: An information-rich autonomous vehicle for high-speed desert navigation," *Journal of Field Robotics*, vol. 23, 2006, pp. 777-810.

[9] A. Bemporad, M. Morari, V. Dua, and E. Pistikopoulos, "The explicit linear quadratic regulator for constrained systems," *Automatica*, vol. 38, 2002, pp. 3-20.

[10] T. Tsukagoshi and H. Wakaumi, "Highly-reliable semi-autonomous vehicle control on lattice lane," *Proceedings. IROS '90. IEEE International Workshop on Intelligent Robots and Systems '90. Towards a New Frontier of Applications, 3-6 July 1990*, New York, NY, USA: IEEE, 1990, pp. 731-8.

[11] M. Netto, J. Blosseville, B. Lusetti, and S. Mammar, "A new robust control system with optimized use of the lane detection data for vehicle full lateral control under strong curvatures," *ITSC 2006: 2006 IEEE Intelligent Transportation Systems Conference, Sep 17-20 2006*, Piscataway, NJ 08855-1331, United States: Institute of Electrical and Electronics Engineers Inc., 2006, pp. 1382-1387.

[12] A. van der Horst, "A time-based analysis of road user behavior in normal and critical encounters," Ph.D. Thesis, Delft University, Delft, The Netherlands, 1990.

[13] R. Fuller, "Determinants of time headway adopted by truck drivers," *Ergonomics*, vol. 24, 1981, pp. 463-474.

[14] A. Polychronopoulos, M. Tsogas, A. Amditis, U. Scheunert, L. Andreone, and F. Tango, "Dynamic situation and threat assessment for collision warning systems: The EUCLIDE approach," *2004 IEEE Intelligent Vehicles Symposium, June 14,2004 - June 17,2004*, Parma, Italy: Institute of Electrical and Electronics Engineers Inc., 2004, pp. 636-641.

[15] G. Engelman, J. Ekmark, L. Tellis, M.N. Tarabishy, G.M. Joh, R.A. Trombley, and R.E. Williams, "Threat level identification and quantifying system," U.S. Patent US 7034668 B2, April 25, 2006.

[16] S.J. Anderson, S.C. Peters, T.E. Pilutti, and K.D. Iagnemma, "Design and Development of an Optimal-Control-Based Framework for Trajectory Planning, Threat Assessment, and Semi-Autonomous Control of Passenger Vehicles in Hazard Avoidance Scenarios," *Proceedings of the 14th International Symposium on Robotics Research*, Lucerne, Switzerland: 2009.

[17] L. Guo, J. Wang, and K. Li, "Lane keeping system based on THASV-II platform," *IEEE International Conference on Vehicular Electronics and Safety, ICVES 2006, Dec 13-15 2006*, Piscataway, NJ 08855-1331, United States: Institute of Electrical and Electronics Engineers Computer Society, 2006, pp. 305-308.

[18] Z. Zomotor and U. Franke, "Sensor fusion for improved vision based lane recognition and object tracking with range-finders," *Proceedings of the 1997 IEEE Conference on Intelligent Transportation Systems, ITSC, Nov 9-12 1997*, Piscataway, NJ, USA: IEEE, 1997, pp. 595-600.

[19] S.J. Anderson, S.C. Peters, T.E. Pilutti, and K. Iagnemma, "An Optimal-Control-Based Framework for Trajectory Planning, Threat Assessment, and Semi-Autonomous Control of Passenger Vehicles in Hazard Avoidance Scenarios," *International Journal of Vehicle Autonomous Systems*, vol. (in press).

[20] P. Falcone, F. Borrelli, J. Asgari, H.E. Tseng, and D. Hrovat, "Predictive active steering control for autonomous vehicle systems," *IEEE Transactions on Control Systems Technology*, vol. 15, 2007, pp. 566-580.

[21] C.G. Prevost, A. Desbiens, E. Gagnon, and D. Hodouin, "UAV optimal cooperative target tracking and collision avoidance of moving objects," P.O. Box 211, Amsterdam, 1000 AE, Netherlands: Elsevier, 2008.